

https://doi.org/10.1070/QEL18040

Thermoelastic stresses in high-power CW diode laser arrays assembled on CuW and AlN submounts

V.P.Gordeev, V.A. Oleshchenko, V.V. Bezotosnyi

Abstract. **Comparative results are presented of 3D-calculation for thermoelastic stress (TES) profiles in diode laser arrays (LDAs) assembled on CuW and AlN submounts (temperature compensators) and operating at a continuous-wave (CW) thermal power load of up to 220 W. For the first time, the simulation has revealed substantial differences in the maximal TES values for the arrays assembled on CuW and AlN submounts, as well as pronounced features of TES distribution in LDA assemblies, in particular, near the rear (highly reflecting) mirror of the laser diode cavity in similar geometries of temperature compensators. Results of the numerical simulation qualitatively agree with thorough measurements of spectral distributions over the LDA emitting aperture. The obtained results are interesting for mastering the production technologies of high-power devices aimed at improving their output parameters and service life.**

Keywords: *diode laser array, temperature compensator, thermoelastic stresses.*

1. Introduction

High power diode laser arrays (LDAs) and laser diode matrices (LDMs) possessing high efficiency, reliability, and ease of employment are widely used to pump solid-state lasers and metal vapour lasers, as well as in material treatment, navigation, physical researches, etc. A striking example of such an employment is direct laser treatment of materials: welding, cutting, hardening, surface cleaning, etc. However, in the radiation brightness, LDAs and LDMs rank noticeably below diode-pumped lasers. Nevertheless, with modern methods for summing radiation from LDAs and LDMs, the brightness of such a synthesised beam may be comparable with that of solid-state lasers. The systems utilising the summed radiation from highly efficient and compact LDAs and LDMs [1–3] have attractive characteristics and compete with solid-state lasers in certain applications. For example, the use of LDAs in schemes with spectral summation [4] made it possible to reach a record power of above 4.6 kW. Obtaining high output characteristics of laser systems based on LDAs and LDMs directly depends on the output characteristics of each laser unit.

V.P.Gordeev, V.A. Oleshchenko, V.V. Bezotosnyi P.N. Lebedev Physical Institute of the Russian Academy of Sciences, Leninsky prosp. 53, 119991 Moscow, Russia;
email: vs.gordeev@yandex.ru, bezotosnyjvv@lebedev.ru

Received 21 February 2022
Kvantovaya Elektronika **52** (5) 443–448 (2022)
Translated by N.A. Raspopov

Substantial obstacles in reaching a record-high output power and radiation brightness with provided prescribed homogeneity of spectral parameters, polarisation, reliability, and service life of all system elements are nonuniform thermal fields of an LDA laser crystal as well as fields of thermoelastic stresses (TES's). In our opinion, the latter have not been studied sufficiently.

Submounts (intermediate heat-conducting elements between a laser crystal and the main heatsink) made of CuW and AlN are most widely used in high-power single laser diodes (LDs) and monolithic LDAs. In the literature, for such submounts, there is no exact and detailed description of the processes leading to inhomogeneous thermal fields, radiation spectra, and polarisation, which is explained by hard efforts needed for developing the required 3D models and performing a complicated analysis of the obtained results. These materials have a substantially lower heat conductivity as compared to copper, and there are no comparative data on absolute values and distribution character of TES's in LD and LDA chips. Consequently, the influence of TES' on the reliability and service life of such devices cannot be estimated, and it is impossible to determine optimal parameters of a laser assembly and guaranteed 'endurance' range of heat loads, which is actual for correct prediction of a service life of emitters in the CW regime.

TES's arising in high-power LDs and LDAs, as in any high-power hybrid device, are due to differences as in the elastic constants of employed heterostructure materials, submounts, solders, and heatsink elements, and so in their temperature dependences, which results in inhomogeneous heating of the device in the operation regime. The main mechanisms of TES manifestation can be classified as follows: 'embedded' stresses in heterostructures, related to mismatched crystal lattice parameters of semiconductor layers with various compositions and to different coefficients of thermal expansion (CTEs) and different CTE dependences; stresses arising during chip packaging, especially actual in technologies with the employment of so-called solid and high-temperature AuSn solder; stresses of the 'operation regime', which arise due to inhomogeneous heating of the laser crystal.

Papers [5–8] describe LDAs operating in a CW and quasi-cw (QCW) regimes and partially investigate the features of output radiation in these regimes, which are presumably related to TES's. Simulation results confirmed inhomogeneities in temperature distribution profiles and TES's in the active medium. In addition, the influence of the chip material, heatsink, and solder has been revealed at various powers of thermal load on a laser crystal. In some works [9–13], the influence of TES's on the polarisation of output radiation and inhomogeneity of its distribution over

the aperture was established. It was shown [10, 14] that a high TES level may result in voids inside solder, which, in turn, may be the reason for inhomogeneous heat removal from an LDA chip. 'Hot' points are produced, which lead to inhomogeneous distribution of the power and spectrum over the width of the emitting aperture and, thus, reduce the emitter reliability.

As known, tension or compression TES's in heterostructures change relative positions of sub-band energy levels of light and heavy holes and, thus, affect the output radiation polarisation [14]. Negative effects due to inhomogeneous heat removal and TES-related factors are reduced by using the chip-on-substrate (COS) technologies in the process of assembling laser chips. In these technologies, a submount is fabricated from a material that is CTE-matched with the laser crystal.

In this work, we present the most interesting results on numerical 3D simulation of CW LDAs arranged on CuW and AlN submounts, which are, in turn, placed on standard copper heatsink elements of CS-mount type. In this case, the LDA limiting thermal load power P_{TL} equal to 220 W is determined as follows

$$P_{TL} = P_{EL}(1 - \eta_{tot}), \quad (1)$$

where P_{EL} is the electric power supplied into the LDA, and η_{tot} is the total efficiency of the array. In addition, for comparison, experimental data on a typical spectrum profile for LDA output radiation over the width of the output aperture are presented and analysed.

2. Simulation

The calculation 3D model considers a typical, COS-assembled, CW LDA crystal fabricated from a heterostructure on a GaAs substrate (λ = 808 nm), with an aperture of 10 mm, a cavity length of 2 mm, and a thickness of 0.12 mm. It is comprised of 47 emitting clusters (emitters) with the filling factor FF = 50%. The thickness of CuW or AlN submounts is 300 μm. In the model, LDA chips are attached to submounts with an AuSn-solder, and the submounts with chips are placed on heatsink elements with a PbSn-solder. In the model, the thickness of the AuSn-solder used for placing chips to submounts varies in the range from 2.5 to 5 μm, and the thickness of the PbSn-solder varies from in the range 5 to 10 μm. The power of the instantaneous thermal load varies from 20 to 220 W. The bottom face of the heatsink is kept at a constant temperature of 293 K. The CS-mount is screwed to a base thermostabilised heatsink through regular holes in the casing. The simulation was performed with the help of COMSOL Multiphysics software. Parameters of the materials used in the simulation are given in Table 1.

Table 1. Parameters of the used materials.

Material	Young modulus /GPa	TEC/10^{-6} m K^{-1}	Poisson ratio
GaAs	86	5.7	0.31
20Au – 80Sn	68	16	0.405
39Pb – 61Sn	40	26	0.4
CuW	260	7	0.3
AlN	348	4.6	0.27
Cu	128	16.5	0.36

One can see from the Table that CTE of CuW is greater, and CTE of AlN is smaller than that of GaAs, the Young's moduli of submount materials being substantially greater than those of GaAs. We will show below that differences in the elastic constants, especially in CTE, lead to various effects under thermal expansion and compression of crystal–solder–submount sandwiches in the process of assembly thermocycling with heating and cooling. This, correspondingly, results in a substantial difference in elastic stress images of 3D fields in cases of CuW or AlN submounts.

Several principally important cross sections of the 3D model have been chosen for presenting simulation results for thermoelastic stresses arising in laser chips assembled on CuW and AlN submounts and for revealing the general picture of TES distribution over the whole body of the laser assembly. These cross sections are: a plane in the active layer,

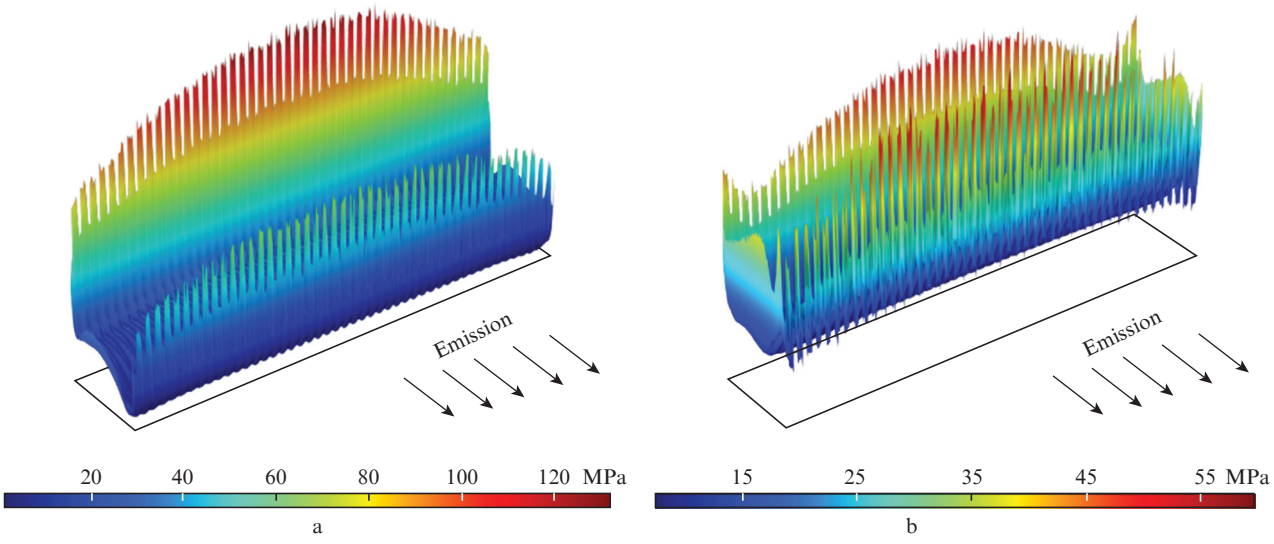

Figure 1. (Colour online) Profiles of mechanical stresses in an active layer of the laser crystal assembled on a (a) CuW and (b) AlN submounts at a thermal load power of 220 W.

a layer between the crystal and submount, a plane inside submount, and a layer between the submount and heatsink.

Active layer. In the simulation model, the active layer is considered as a plane due to its small thickness as compared to that of the LDA crystal (a typical thickness of an active layer in modern quantum-well heterustructures is about 100 nm). In this model layer, where charge carriers recombine and heat is released, the emitting units (clusters) are presented by rectangles. All the dissipated power P_{TL} is released through the emitter areas in equal parts for each of the 47 clusters.

The active layer is the most interesting for studying, because thermoelastic stresses revealed in it are the most indicative of the spectrum and polarisation variations in the output radiation. Figure 1 presents amplitude distributions of von Mises thermoelastic equivalent stresses σ_{VM} for CuW and AlN submounts in the plane cross section of a 3D image of the active layer, which are given by

$$\sigma_{VM} = \sqrt{\frac{1}{2}[(\sigma_h - \sigma_r)^2 + (\sigma_h - \sigma_a)^2 + (\sigma_a - \sigma_r)^2 + 3\tau^2]}, \quad (2)$$

where σ_h, σ_r, σ_a, and τ are the ring, radial, axial, and tangential stresses, respectively. From Fig. 1 one can see that the greatest stress (~120 MPa) is attained at the rear cavity mirror of a CuW submount, whereas for an AlN submount this value is 2.7 times less (~44 MPa). In this case, the average value of stresses in the considered plane is ~20 MPa, and the most intensive stresses are observed in a thin layer near the highly reflecting rear mirror.

Such noticeable differences in stress values for the materials considered are explained by CTE ratios for submount materials and laser crystal, as well as by the geometry of an assembled sandwich. The high values of thermoelastic stresses at LDA edges can be explained by so-called edge effects, LDA and submount geometry, and differences in thermal and mechanical characteristics of materials involved. A substantial asymmetry of the stress profile along the cavity is due to the fact that the LDA output mirror is arranged at a submount edge, whereas, for technical reasons, the rear mirror is at a certain distance from submount rear edge. Finally, a displacement of the free front edge of the submount is greater

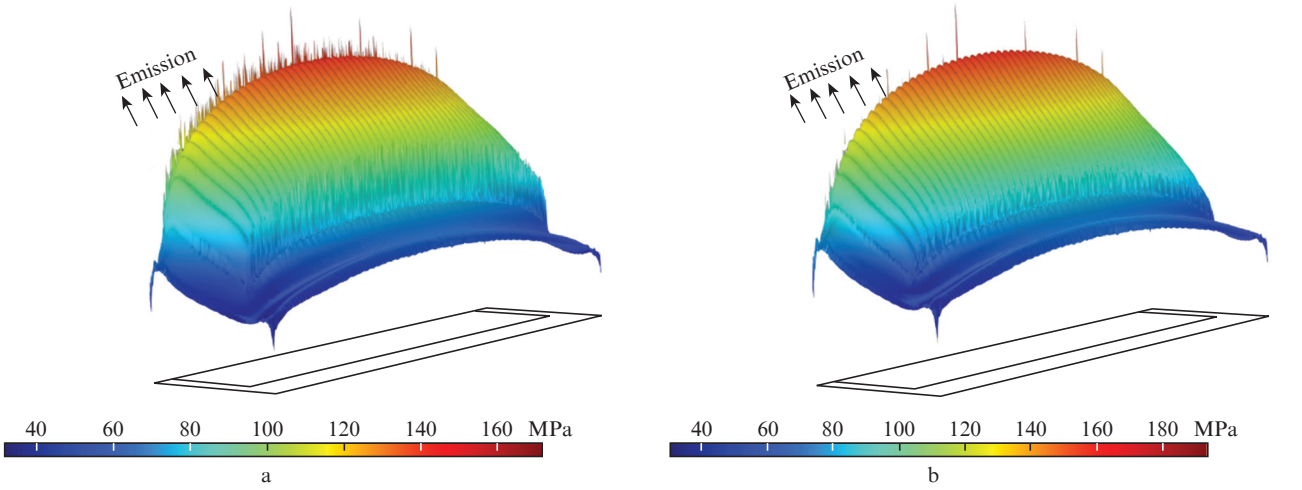

Figure 2. (Colour online) Profiles of mechanical stresses in the solder layer between the laser crystal and (a) CuW and (b) AlN submounts at a thermal load power of 220 W.

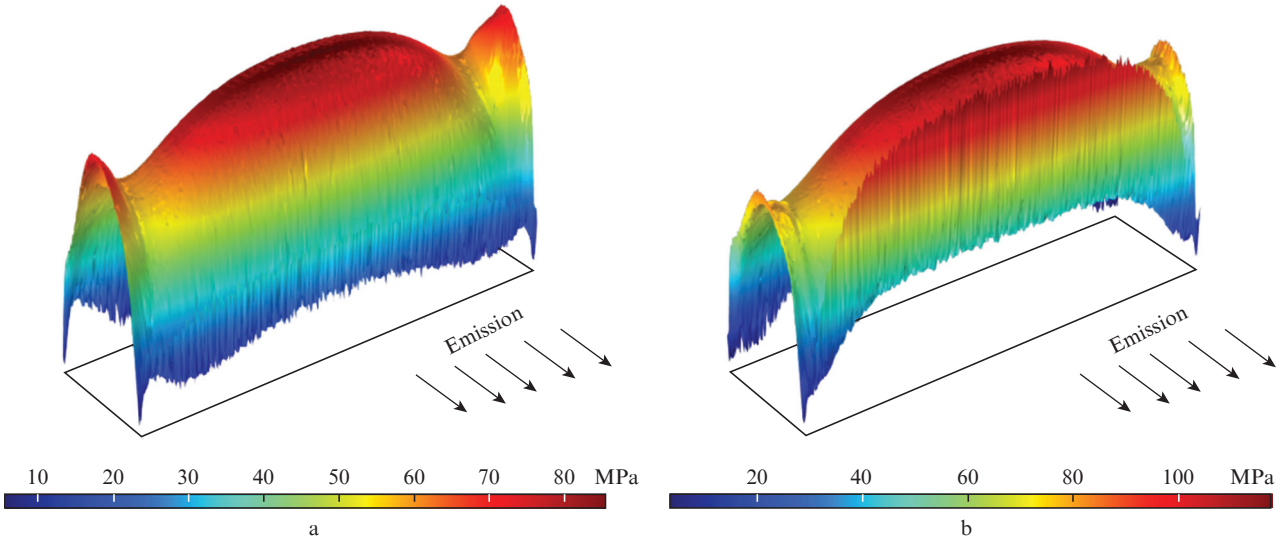

Figure 3. (Colour online) Profiles of mechanical stresses in (a) CuW and (b) AlN submounts at a thermal load power of 220 W.

and, respectively, the stress near the front edge is lower. At the crystal rear edge, the situation is different: a displacement of the submount material near the rear mirror is damped by the volume of 'free' material residing outside the crystal. Hence, stresses at the rear mirror are substantially higher.

Solder layer between crystal and submount. Figure 2 presents distributions of stress amplitudes σ_{VM} for CuW and AlN submounts in the solder layer between the crystal and submount. For clearness, a view from the rear mirror is presented to make the profile details visible.

One can see from Fig. 2 that the profiles obtained principally differ from those in Fig. 1. The greatest TES values are observed near the output mirror rather than near rear mirror, similarly to the case of the cross-section plane in the active layer. In this case, the strongest stresses (~180 MPa) are reached with the AlN submount in contrast to ~160 MPa in the case of the CuW submount. In addition, a sharp change in stresses is observed in the domain under the LDA crystal: ~20 MPa for the CuW submount and ~10 MPa for AlN.

Submount. Figure 3 presents amplitude distributions for stresses σ_{VM} in a body of the submount. Typical TES profiles in both submounts are rather similar. One can see specific profile features at edges. They are related both to geometries of submounts and of the LDA crystal arranged on the latter and to the set of parameters presented in Table 1. Note that the strongest stresses arise in the AlN submount, the stress distribution having the more pronounced maximum at the centre and less distinct spikes at LDA chip edges.

Solder layer between submount and heatsink. This layer is specific in that materials with mostly distinct CTEs are on both sides of it (see Table 1). Figure 4 shows amplitude distributions of stresses σ_{VM} for CuW and AlN submounts in the solder layer between the submount and heasink. For ease of analysis, the distributions are shown from the side of the front mirror at a certain angle.

One can see that the strongest stresses in the solder layer are observed not far from the rear mirror. However, while approaching the mirror, the stresses decrease so that near the mirror the fall is approximately 30 and 50 MPa for CuW and AlN submounts, respectively. The maximal TES value for the AlN submount (~120 MPa) is twice that for the CuW submount (~60 MPa).

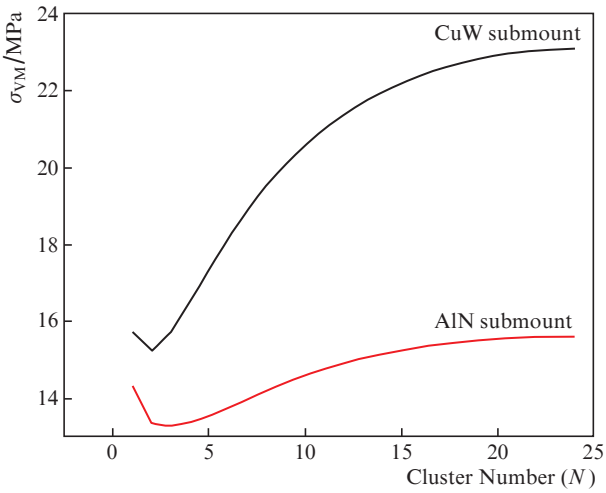

Figure 5. (Colour online) Profiles of mechanical stresses averaged over clusters in the plane of the active layer for CuW and AlN submounts at a thermal load power of 220 W. A half-aperture of the LDA is shown, because the distribution for 47 clusters is symmetrical relative to the central cluster.

3. Analysis of the calculation results

Analysis of the results in Fig. 1 shows that there are substantial differences both in the absolute values and in the distribution character of TES's arising in the process of LDA arrangement on AlN and CuW submounts. Nevertheless, the distribution profiles for average stresses over the clusters of half the emitting aperture in the plane of the active layer (Fig. 5) are similar for both submount types: the strongest stresses are observed at the aperture centre and fall at aperture boundaries. Stress distributions are symmetrical relative to the aperture centre and have the maximum at the centre and spikes at edges of the LDA chip. The stress at the distribution maximum for the CuW submount is substantially greater than for the AlN submount.

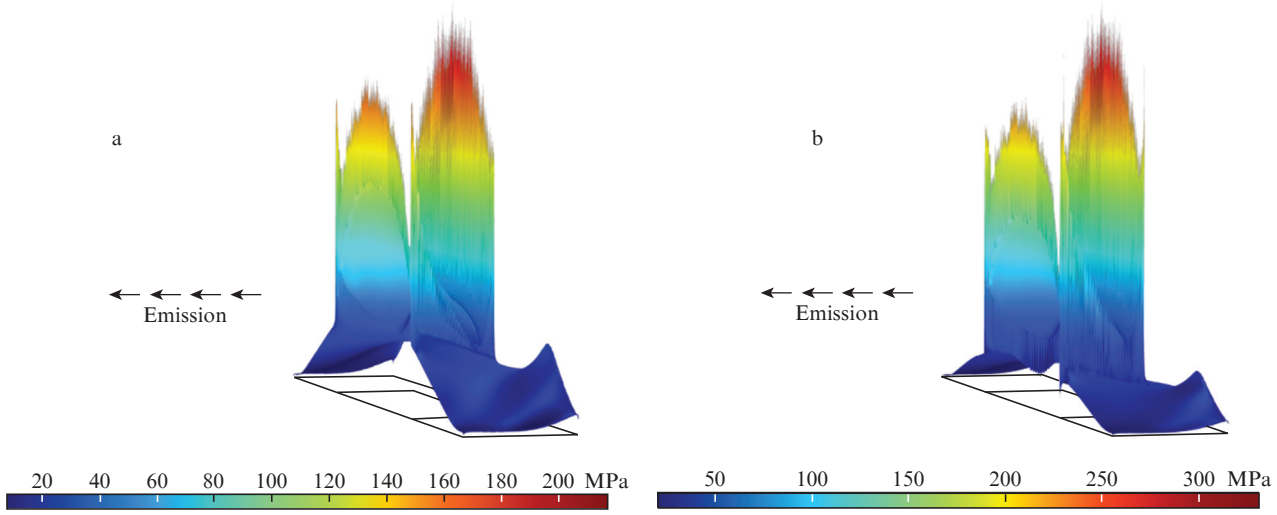

Figure 4. (Colour online) Profiles of mechanical stresses in the solder layer between the heatsink and (a) CuW (a) and (b) AlN submounts at a thermal load power of 220 W.

It worth noting that in other considered cross sections of the assembly the TES value with AlN was noticeably greater than that with CuW. This feature of the TES distribution in a complicated 5-layer construction comprising a COS placed on a copper CS mount presents a principal possibility to reduce effective averaged stresses in the active layer while employing the AlN submount, which is interesting for assembling technologies. This is why this material is now frequently employed for assembling single LDs and LDAs, despite of its dielectric properties.

4. Experiment

A direct experimental measurement of thermoelastic stresses in LDAs is difficult. However, measurements of laser parameters implicitly dependent on a stress value are possible. One of such parameters is the radiation spectrum (in our case, measurement of the spectral distribution over the width of the LDA emitting aperture), because the radiation wavelength depends on a width of the forbidden band, which, in turn, depends on a value of mechanical stresses. In view of the fact that the distribution profile of released heat in the LDA operation regime substantially affects the spectral distribution over aperture, such measurements were taken in the QCW regime at a small current excess over the generation threshold. Figure 6 presents the measured distribution of the wavelength of the LDA spectrum envelope maximum over the emitting aperture in the QCW regime at a comparatively low thermal load power.

The general character of the spectral distribution in Fig. 6 is such that the wavelength (except for the dips at LDA longitudinal coordinates 1.9 and 8.8 mm) is greater as the emitting cluster becomes closer to the LDA edge, the central part of the distribution being actually a plateau. The latter fact can be related to a temperature distribution profile, which has a maximum at a centre of the emitting aperture that causes peripheral clusters to more intensively heat the central clusters. This spectral distribution principally agrees with results of the simulation model for the TES distribution with maxima at LDA edges. This also qualitatively agrees with the calculation data from Fig. 1 where dips in the TES distribution are observed at LDA edges.

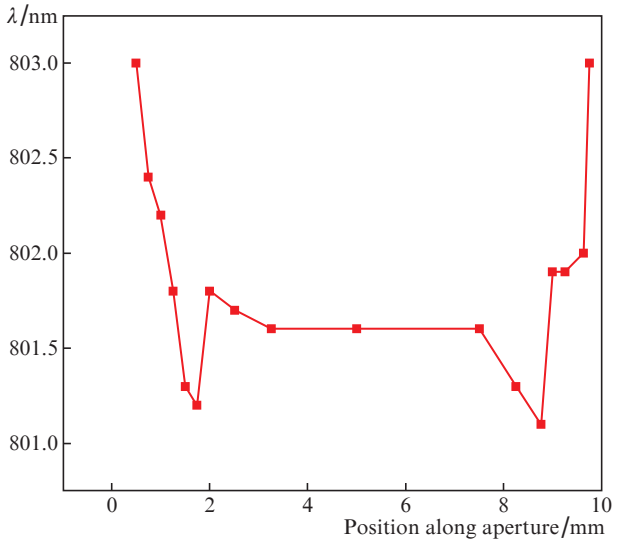

Figure 6. (Colour online) Typical spectral distribution of LDA emission over the longitudinal coordinate of the aperture at a moderate thermal load power of 10 W.

5. Discussion of the obtained results and conclusions

TES 3D fields are obtained, which are presented in the form of various cross sections of the LDA design that employs two the most actual submount types based on CuW and AlN. The simulation results, implicitly confirmed in the experiment, along with the results from papers [7–10], show that effective TES distributions in investigated laser crystals emitting at a wavelength of 808 nm lead to a noticeable shift of the maximum of the spectrum envelope of separate clusters and correspond to compression stresses in investigated LDA samples.

Absolute values of stresses arising due to various mechanisms of TES origin, and the corresponding 3D distributions are calculated in a five-layer structure of an LDA assembly. It was confirmed that in the operation regime, the maximal values of thermoelastic stresses are substantially less than those arising in the process of laser chip assembling because the temperature variation observed over the emitting aperture is substantially less than thermocycling temperature drops in the course of assembling. Calculations show that in the active layer of the LDA, the effective averaged stress values in the devices with AlN submounts are substantially less than in devices with CuW submounts, which is an obvious advantage of AlN.

Nevertheless, CuW in contrast to AlN is a current-conducting material, and this is an obvious advantage for its employment in an LDA design. In this case, it is easy to provide a low-resistance positive high-current contact, whereas in the case of AlN, a substantial thickness of the metallisation layer is needed for supplying the current to the p-type of a laser chip. The latter factor increases the thermal resistance of the assembly and may cause problems with a long-term stability of LDA operation due to the metallisation creep effect that is accelerated by a high-density pump current.

The obtained results have revealed interesting features of TES distributions over the emitting aperture and LDB cavity length for two considered types of submounts, in particular, a high stress intensity near the highly reflecting rear mirror. This fact should be taken into account both in already used LDAs in the assembling and mirror deposition technologies and in the development of new LDA designs of enhanced power, reliability, and service life in CW and QCW regimes.

The calculation 3D model developed for the analysis of thermoelastic stresses in multilayer constructions of high-power LDs and LDAs for the first time suggests a principal possibility to shift the TES maximum from the active layer to passive layers, which seems rather attractive and requires further experimental tests. The calculation results have also shown that a further more detailed study of the LDA assembling process from the viewpoint of arising TES's in high-power laser crystals is important for improving technologies of high-power LDB production.

References

1. Xunchun Lin, Guyi Lin, Pengfei Zhao, Lirong Wang, Haijuan Yu. *Opt. Laser Technol.*, **116**, 219 (2019).
2. Sun Fangyuan, Shu Shili, Hou Guanyu, Wang Lijie, Zhang Jun, Peng Hangyu, Tian Sicong, Tong Cunzhu, Wang Lijun. *IEEE J. Quantum Electron.*, **55** (1), 1 (2019).
3. Zeng Deng, Jun Shen, Wenchi Gong, Wei Dai, Maoqiong Gong. *Int. J. Heat Mass Transfer*, **134** (2), 41 (2019).
4. Robin K. Huang, Bien Chann, James Burgess, Bryan Lochman, Wang Zhou, Mike Cruz, Rob Cook, Dan Dugmore, Jeff Shattuck, Parviz Tayebati. *Proc. SPIE*, **9730**, 97300C-1 (2017).
5. Bezotosnyi V.V., Kozyrev A.A., Kondakova N.S., et al. *Vestnik FIAN*, **43** (12), 369 (2016).
6. Bezotosnyi V.V., Kozyrev A.A., Kondakova N.S., et al. *Quantum Electron.*, **47** (1), 5 (2017) [*Kvantovaya Elektron.*, **47** (1), 5 (2017)].
7. Bezotosnyi V.V., Gordeev V.P., Krokhin O.N., Mikaelyan G.T., Oleshchenko V.A., Pevtsov V.F., Popov Yu.M., Cheshev E.A. *Quantum Electron.*, **48** (2), 115 (2018) [*Kvantovaya Elektron.*, **48** (2), 115 (2018)].
8. Bezotosnyi V.V., Gordeev V.P., Oleshchenko V.A. *Quantum Electron.*, **48** (6), 502 (2018) [*Kvantovaya Elektron.*, **48** (6), 502 (2018)].
9. Hongyou Zhang, Chung-En Zah, Xingsheng Liu. *Proc. SPIE*, **10900**, 109000T (2019).
10. Zhiqiang Nie, Yao Lu, Tianqi Chen, Yu Zhang, Dehai Wu, Mingpei Wang, Lingling Xiong, Xiaoning Li, Zhenfu Wang, Xingsheng Liu. *IEEE Trans. Compon. Packag. Manuf. Technol.*, **8** (5), 818 (2018).
11. Zhu H., Liu K., Xiong C., Feng S., Guo C. *Microelectron. Reliab.*, **55** (1), 62 (2015).
12. Scholz C. *Thermal and Mechanical Optimisation of Diode Laser Bar Packaging* (Norderstedt: Books on Demand GmbH, 2007).
13. Mikaelyan G.T. *Quantum Electron.*, **36** (3), 222 (2006) [*Kvantovaya Elektron.*, **36** (3), 222 (2006)].
14. Bogdanov E.V., Kolokolov K.I., Minina N.Y., in *Physics, Chemistry and Application of Nanostructures: Reviews and Short Notes to Nanomeeting 2017* (World Scientific, 2017) pp 475 – 478.